Latin American Journal of Solids and Structures
www.lajss.org

Crashworthiness Analysis of S-Shaped Structures Under Axial Impact Loading

Abstract

To mitigate shock forces in collision events, thin-walled members are used as energy absorber. In this article, crashworthiness of single-cell and multi-cell S-shaped members with various cross-sections including triangular, square, hexagonal, decagon and circular were investigated under axial dynamic loading using finite element code LS-DYNA. Furthermore, crashworthiness of the S-rails with the same outer tubes and different inner ones was studied as well. The multi-cell members employed in this task were double-walled tubes with several ribs connecting the inner and outer tubes together. Modified multi criteria decision making method known as complex proportional assessment (COPRAS) was used to rank the members using three conflicting crashworthiness criteria namely specific energy absorber (SEA), peak crash force (F_{max}) and crash force efficiency (CFE). Moreover, the multi-cell S-shaped members were found to perform better than single-cell ones in terms of crashworthiness. In addition, the multi-cell S-rail with decagonal cross-section was found as the best energy absorber, and also the S-rail having the same inner and outer tube with decagonal cross-section displayed desirable crashworthiness performance. Optimum geometry of this S-rail was eventually obtained from the parametric study.

Keywords

Multi-cell members, S-rails, axial dynamic loading, crashworthiness, COPRAS.

Sobhan Esmaeili-Marzdashti [a]
Sadjad Pirmohammad [b,*]
Sareh Esmaeili-Marzdashti [c]

[a] Department of Mechanical Engineering, University of Mohaghegh Ardabili, Ardabil, 179, Iran. Sobhanesameili90@gmail.com
[b] Department of Mechanical Engineering, University of Mohaghegh Ardabili, Ardabil, 179, Iran. s_pirmohammad@uma.ac.ir
(* Corresponding Author)
[c] Department of Mechanical Engineering, Polytechnique Montreal, Station Downtown Montreal, Quebec, 6079, Canada. sarehesmaeili84@yahoo.com

http://dx.doi.org/10.1590/1679-78253430

Received 13.10.2016
In revised form 18.02.2017
Accepted 21.02.2017
Available online 04.03.2017

1 INTRODUCTION

The front end part in the vehicles is desired to be folded progressively during car frontal crash so as to absorb more energy and provide safety for the passengers. In order to develop more progressive

folding wrinkles, at the early stage of frontal crash, and to absorb more energy in buckling at the late stage of crash, it is important to improve the crashworthiness of the front end member. Figure 1 shows an example for the possible use of members as energy absorbers in the longitudinal frames of automobiles (Marsolek and Reimerdes, 2004). Designing automotive body structure to achieve maximum safety, as significant vehicle attribute, is an important research field that has received considerable attention (Atahan et al., 2014; Belingardi et al., 2013; Pawlus et al., 2011).

Curved tubes used in the vehicle structures have significant effects on prolonging deformation of the frame (Han and Yamazaki, 2003; Cheon and Meguid, 2004) in the crash events. There are some experimental and numerical studies on the collapse behavior of S-shaped beams which have been done by Ohkami et al. (1990), Abe et al. (1990) and Zhang (2005). They reinforced these beams to promote their energy absorption capacity.

In addition to the energy absorption capacity of the vehicle front end structure, weight is considered to be an important issue attempted to be minimized. Kim and Wierzbicki (2000) have carried out a study by investigating different methods to ameliorate structural crashworthiness of internal members. In another study, Ohkami et al. (1990) experimentally investigated collapse behavior of the thin-walled curved tube with closed-hat section subjected to static and dynamic loading.

Hosseini-Tehrani and Nikahd (2006) employed various arrangements of straight and sidling ribs within the S-shaped tubes so as to achieve the members possessing better crashworthiness performance and higher weight efficiency. Although structural modification has a significant effect on crashworthiness performance and produces light weight tubes, recent studies have revealed that the crashworthiness capacity and weight efficiency can be further improved by applying some materials as well (Hosseini-Tehrani and Nikahd, 2006). In order to increase the weight efficiency of the S-shaped tubes, Kim et al. (2002) have applied aluminum foam filler. Finding an appropriate contact between the wall and foam filler was the advantage of their study.

Several works have been done in recent years on the effect of foam filler on the energy absorption of structures (Reyes et al., 2004; Chen, 2001; Hong et al., 2005; Li et al., 200). Kim and Wierzbicki (2004) studied crushing behavior of S-rails with rectangular cross-section. Their research indicated that the critical aspect ratio of the rectangular cross-section was 1.366. Also, according to their investigation, analytically derived crushing force gave excellent correlation with the finite element results. Khalkhali et al. (2011) made an experimental and numerical investigation on the single-cell S-shaped tubes with square cross-section under quasi-static axial loading. In another work carried out by khalkhali et al. (2013) they derived a closed form solution for calculating crushing force of the S-rails. More recently, Elmarakbi et al. (2011) studied energy absorption capacity of the simple S-shaped members with different cross-section shapes and several inner ribs. Reviewing the literature, as mentioned above, indicates that many investigations have been performed on the S-shaped members. However, some new designs of sectional configurations are presented in the current work.

Therefore, crashworthiness of new designed multi-cell S-shaped members together with the single-cell S-rails was studied under axial impact loading in the present work. These members have included several sectional configurations namely triangular, square, hexagonal, decagon and circular cross-sections. Finite element code LS-DYNA was used to simulate the collapse behavior of these members. In addition, modified multi criteria decision making method namely complex proportional

assessment (COPRAS) was used to rank the considered members from the crashworthiness point of view.

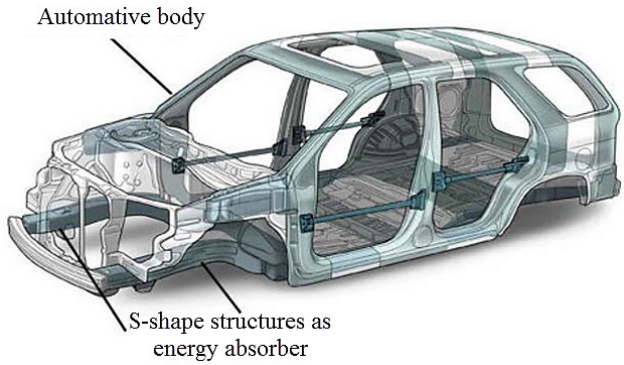

Figure 1: Energy absorbing members used in the automotive body.

2 S-RAIL GEOMETRY AND MATERIAL

This study focuses on the crashworthiness of different single-cell and multi-cell S-shaped tubes. Figure 2 shows the various cross-section configurations namely triangular, square, hexagonal, decagon and circular assumed for the S-shaped members. The single-walled and double-walled S-shaped tubes have been designated as SCTS, SCSS, SCHS, SCDS, SCCS (see Figure 2a) and MCTS, MCSS, MCHS, MCDS, MCCS (see Figure 2b), respectively. The ribs in the double-walled members connected middle of the outer and inner tube sides together. Geometrical model of the S-rail has been depicted in Figure 3, where L, R, ϑ, and t denote the length, radius of curvature, curve angle and wall thickness, respectively. The outer perimeter of all cross-sections was chosen the same and equal with 534 mm. In addition, ratio of the inner tube to the outer one of double-walled members was assumed to be 0.5 as well as the wall thickness of all the tubes shown in Figure 2 was selected 3mm.

Shape of cross-section	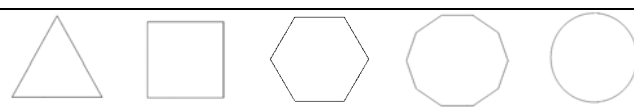				
Designation	SCTS	SCSS	SCHS	SCDS	SCCS
Mass (kg)	4.9	4.9	4.9	4.9	4.9

(a)

Shape of cross-section	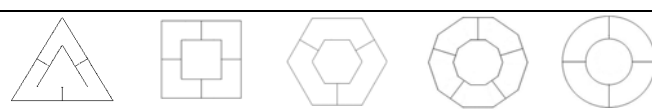				
Designation	MCTS	MCSS	MCHS	MCDS	MCCS
Mass (kg)	8.41	8.72	8.55	9.24	8.95

(b)

Figure 2: Cross-section shapes of (a) Single-cell and (b) multi-cell S-shaped members.

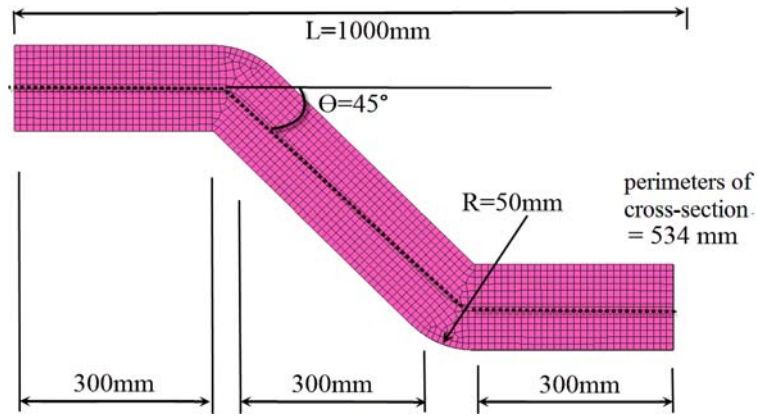

Figure 3: Geometry and dimensions of S-shaped member.

The material of tubes was assumed Aluminum alloy AA6060T4 with Young's modulus E=68.2Gpa, Poisson's ratio υ=0.3, mass density ϱ=2700 kg/m^3, yield strength σ_y = 80MPa and Ultimate strength σ_u =173MPa. The stress-strain curve obtained from the tensile test has been shown in Figure 4. Since, Aluminum alloy is insensitive to the strain rate (Langseth and Hopperstad, 1996); therefore, its effect was ignored in the finite element analyses.

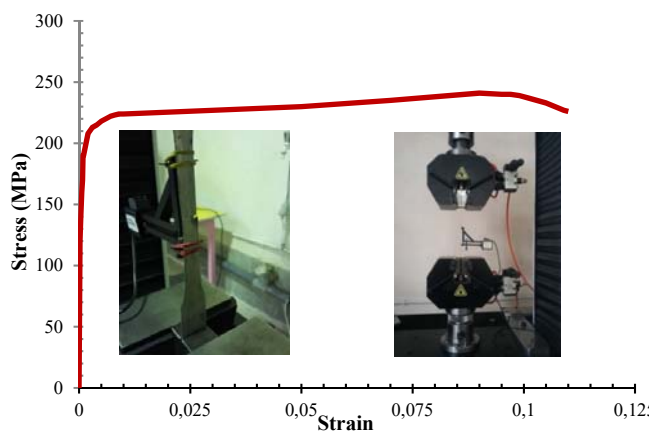

Figure 4: Elastic-plastic stress-strain behavior of Aluminum AA6060.

3 CRASHWORTHINESS CRITERIA

Three important criteria namely specific energy absorption (SEA), peak crash force (F_{max}) and crash force efficiency (CFE) have been used in this paper to assess crashworthiness of the S-shaped members. Equation (1) indicates formula of the SEA which is typically defined as the total strain energy absorbed during the plastic deformation. It is calculated by dividing the energy absorption capacity (EA) during the crushing process to the total mass of member. Thus, an appropriate energy absorber must have higher value of SEA.

$$SEA = \frac{EA}{m} = \frac{\int_0^{\delta} F(x)dx}{m} \tag{1}$$

Where F(x) denotes variations of the instantaneous crushing load and δ is the effective stroke length (Chen and Wierzbicki, 2001), which is taken as 0.4L in this study, and L is the total length of the energy absorbing device.

The average value of F(x), called as the mean collapse load (F_{mean}), is calculated as the ratio of the total energy absorbed by tube to the effective stroke length δ. This parameter is defined as:

$$F_{mean} = \frac{\int_0^{\delta} F(x)dx}{\delta} \tag{2}$$

Another crashworthiness indicator is the crash force efficiency (CFE) which is calculated by the division of the mean collapse load (F_{mean}) to the F_{max} as follows:

$$CFE = \frac{F_{mean}}{F_{\max}} \times 100 \tag{3}$$

4 NUMERICAL ANALYSIS

4.1 Finite Element Modeling

Non-linear finite element code LS-DYNA was employed to study energy absorption capacity and crushing behavior of the S-rails under axial dynamic loading. Geometry of these S-rails was designed in CATIA software, and they were then exported to the post-processor LS-PREPOST in LS-DYANA to analyze the impact problem so that acquire aforementioned crashworthiness criteria. Figure 5 shows schematic of the finite element analysis set-up. A rigid striker with initial velocity of 10 m/s and added mass of 500kg impacted on the S-shaped members axially. This process was modeled using the RIGID WALL_PLANNAR MOVING FORCE command in LS-DYNA. To avoid any movement under the crash, the stationary boundary condition was employed at the end of tubes. Besides, the members were modeled using the quadrilateral four-node shell elements with five integration points through the thickness. The decreased hourglass and integration technique were applied in the analyses to avoid volumetric locking and spurious zero energy deformation cases. Mesh convergence analysis was performed, and the optimal element size was finally found to be 5mm×5mm; while, the element size at the corners was taken finer (about 1mm×1mm). AUTOMATIC-NODE-TO-SURFACE algorithm was used to model the contact between the striker and members. In addition, AUTOMATIC-SINGLE-SURFACE algorithm was used to consider the contact between the S-rail walls to avoid penetrating the walls into together. The friction coefficient of 0.15 was adopted for all the contact conditions (Ahmed et al., 2013). It is also noticed that material of the tubes was modeled by MAT-024 (namely modified-piecewise-Linear-plasticity) in LS-DYNA.

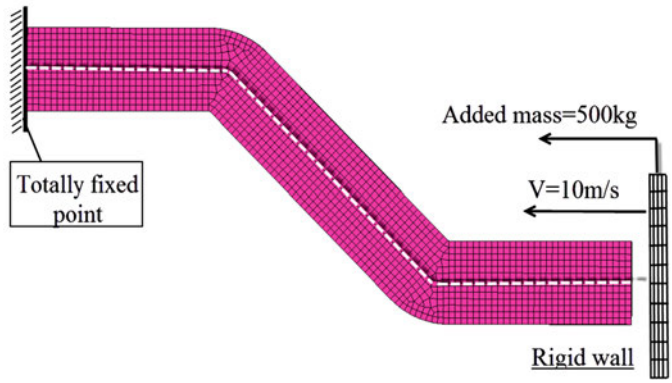

Figure 5: Mesh pattern and boundary conditions applied in the finite element models.

4.2 Validation of FE Simulations

To validate the finite element simulations of the crash problem, experiments were performed on the square tubes using the universal test machine under the longitudinal loading, and they were then simulated in LS-DYNA. The tubes with square cross-section of 40×40mm, the thickness of 2 mm and the length of 90 mm were constrained on the lower part of the fixture; while, the upper part of this fixture crushed 40% of the tube length with a constant displacement rate of 10 mm/min (see Figure 6). These tubes were also simulated in LS-DYNA similar to the experimental conditions mentioned above, and the results have been given in Figure 6 for comparing with the experimental results. As is evident in this figure, there is a satisfied agreement between the two sets of results in terms of deformation modes, force–displacement responses, and crashworthiness indicators. The relative error (R_e) between the three crashworthiness criteria for the numerical ($f_{Num.}$) and experimental ($f_{Exp.}$) results was calculated by the Equation (4).

$$R_e = \left| \frac{f_{Num.} - f_{Exp.}}{f_{Num.}} \right| \tag{4}$$

4.3 Finite Element Results for the Designed S-Rails

Collapse behavior of the S-shaped members with different cross-sections illustrated in Figure 2 was analyzed in LS-DYNA according to the notes mentioned in the section 4.1. Deformation modes of these S-rails have been shown in Figure 7. It is reminded that the striker identically crushed 40 percent of the total length of the S-rails. As is clear from Fig. 7, the plastic hinges (formed at the curved zones of the S-rails due to the global bending mode) absorbed the main kinematic energy of the striker. Force-displacement curves for the studied S-rails have been plotted in Figure 8. From this figure, the force initially increased to reach its maximum value, and then suddenly decreased with a sharp steep due to global bending deformation mode.

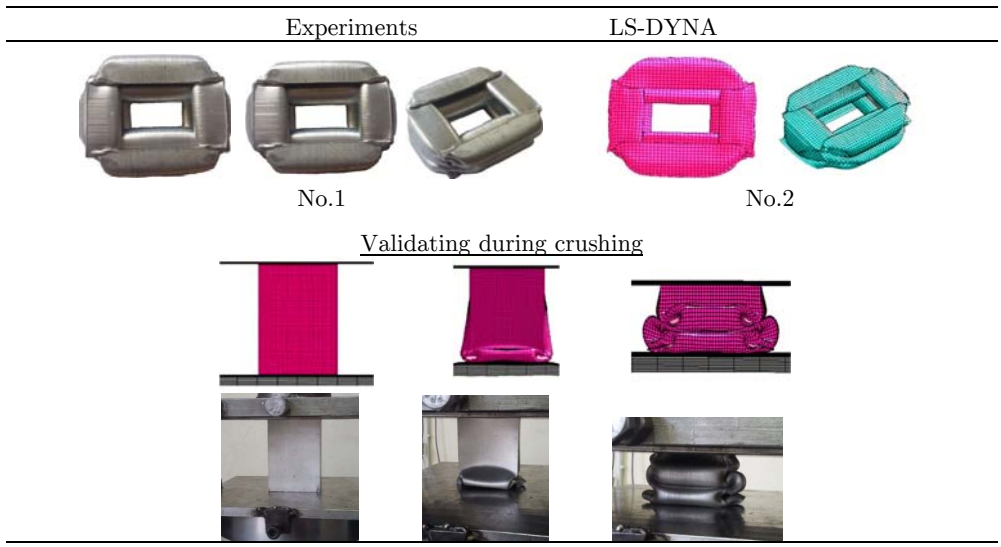

(a)

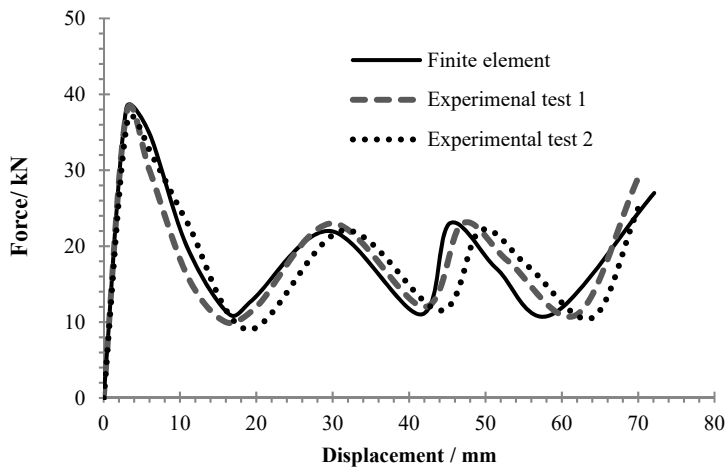

(b)

	EA(kJ)	F_{max}(kN)	CFE (%)
Test1	1.33	37.52	50.41
Test2	1.3	36.81	50.41
FE	1.35	38.09	50.62
$R_{e\ 1}$ (%)	1.48	1.49	0.414
$R_{e\ 2}$ (%)	3.7	3.36	0.414

(c)

Figure 6: Comparison of the experimental and numerical results: (a) deformation modes, (b) force versus displacement curves, (c) crashworthiness indicators.

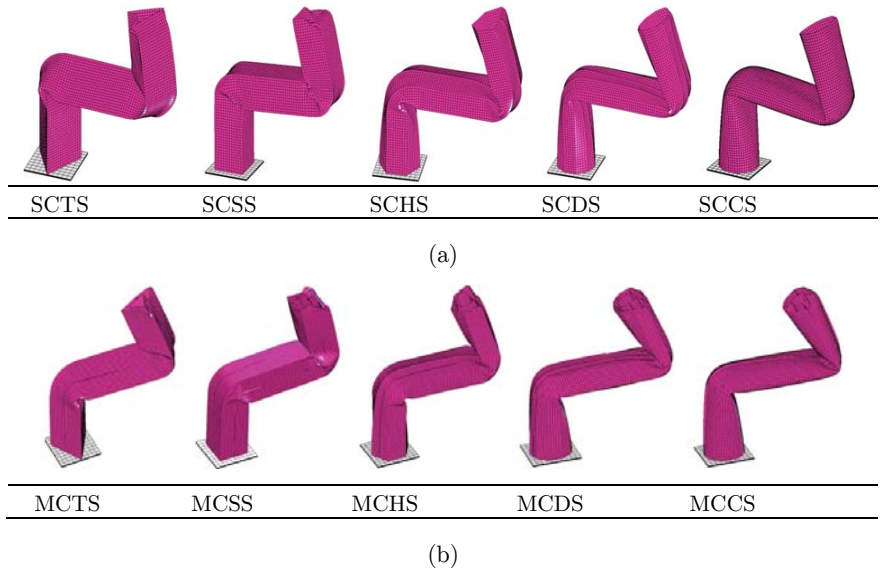

Figure 7: Deformed modes of (a) single-cell and (b) multi-cell S-shaped members.

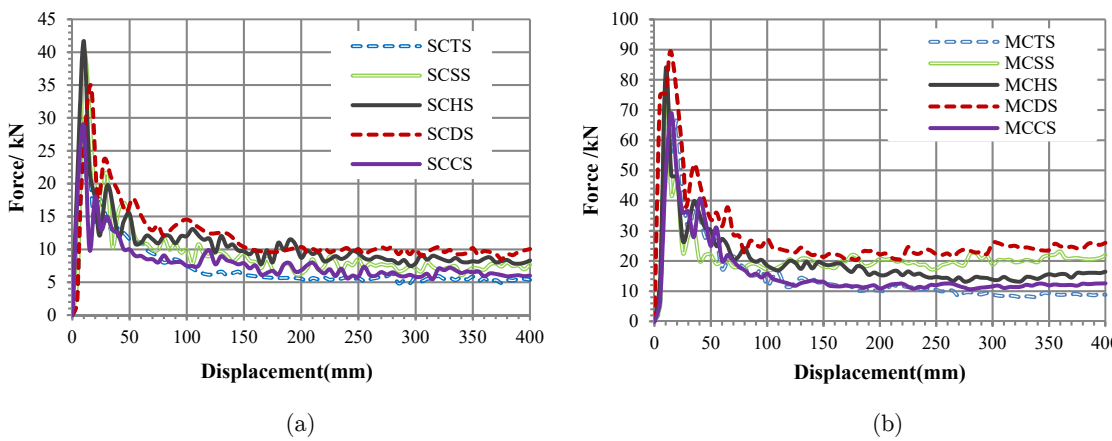

Figure 8: Force-displacement curves for (a) the single-cell and (b) multi-cell tubes.

The SEA calculated from the Figure 8 has been plotted in Figure 9a. From which it is clear that the decagonal and triangular cross-sections had the highest and the lowest values of SEA, respectively compared to the other cross-sections. However, the ranking in terms of the SEA value is: SCDS> SCHS> SCSS> SCCS> SCTS. The amount of energy absorption for the single-cell decagonal (SCDS) and hexagonal tubes (SCHS) were 0.855kJ/kg and 0.81kJ/kg, respectively which were found to be the best energy absorbing devices. This result exhibits that the energy absorption generally goes up by increasing sides of the cross- section.

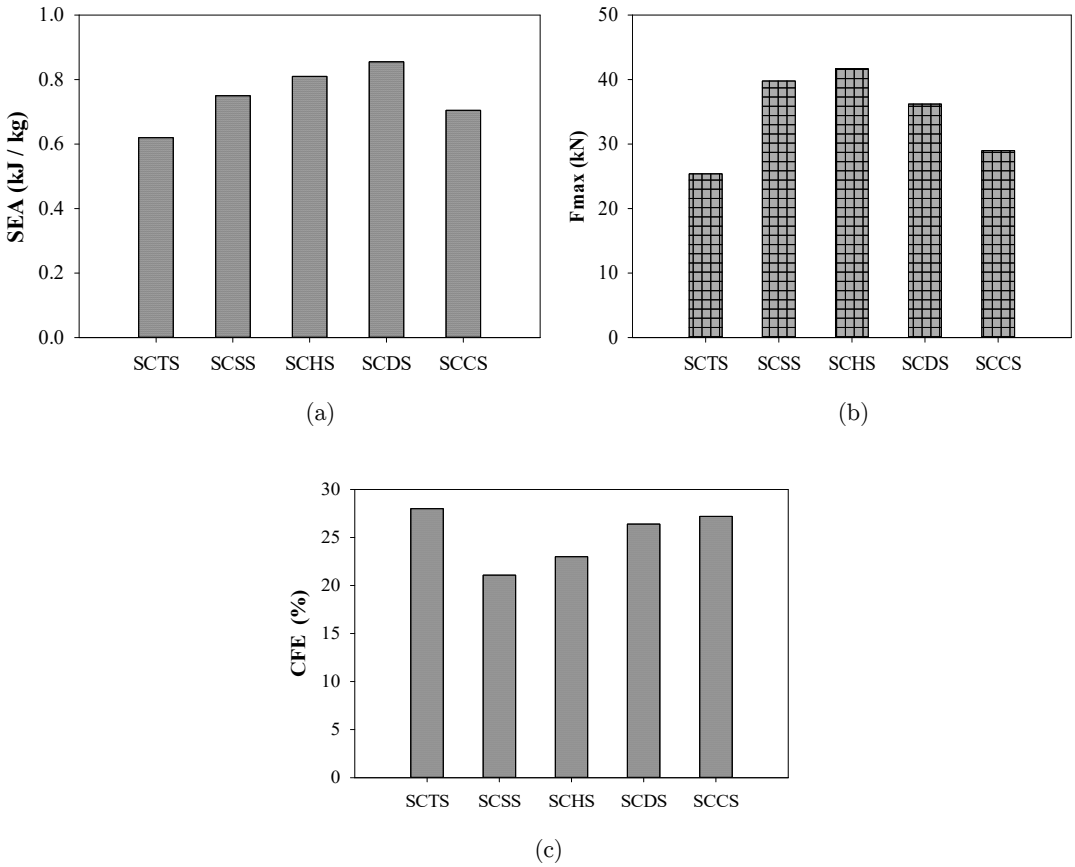

Figure 9: Crashworthiness indicators for the single-cell S-rails: (a) SEA, (b) F_{max}, and (c) CFE.

Figure 9b presents values of the F_{max} for the considered S-rails. As is evident from this figure, the single-cell S-rails were ranked as follows: SCHS> SCSS> SCDS> SCCS> SCTS. Therefore, the single-cell hexagonal (SCHS) and square (SCSS) members possessed higher peak crash force values which could be detrimental to the vehicle safety. Results for the crash force efficiency (CFE) have been given in Figure 9c. By comparing values of the CFE, it is seen that the SCTS, SCCS and SCHS members have greater values among the single-cell structures.

Results of the three mentioned criteria for the multi-cell S-rails have been given in Figure 10. The ranking in order of the SEA values were obtained as: MCDS> MCSS> MCHS> MCTS> MCCS according to Figure 10a. Comparing the results of single-cell tubes with the multi-cell ones indicates that addition of the ribs to the double-walled S-rails contributed to the improvement of SEA values due to developing the plastic hinges at the corners. The multi-cell tube with decagonal cross-section (MCDS) has greater ability to absorb energy than MCHS tubes and MCSS tubes.

Initial peak force causes severe injury or damage to the people or automobile structures so it is significantly undesirable in crash performance. The results for this negative crashworthiness indicator have been given in Figure 10b for the multi-cell S-rails. Results for the crash force efficiency

(CFE) have been given in Figure 10c. By comparing values of the CFE, it is clear that the SCDS had the highest value among the considered multi-cell structures.

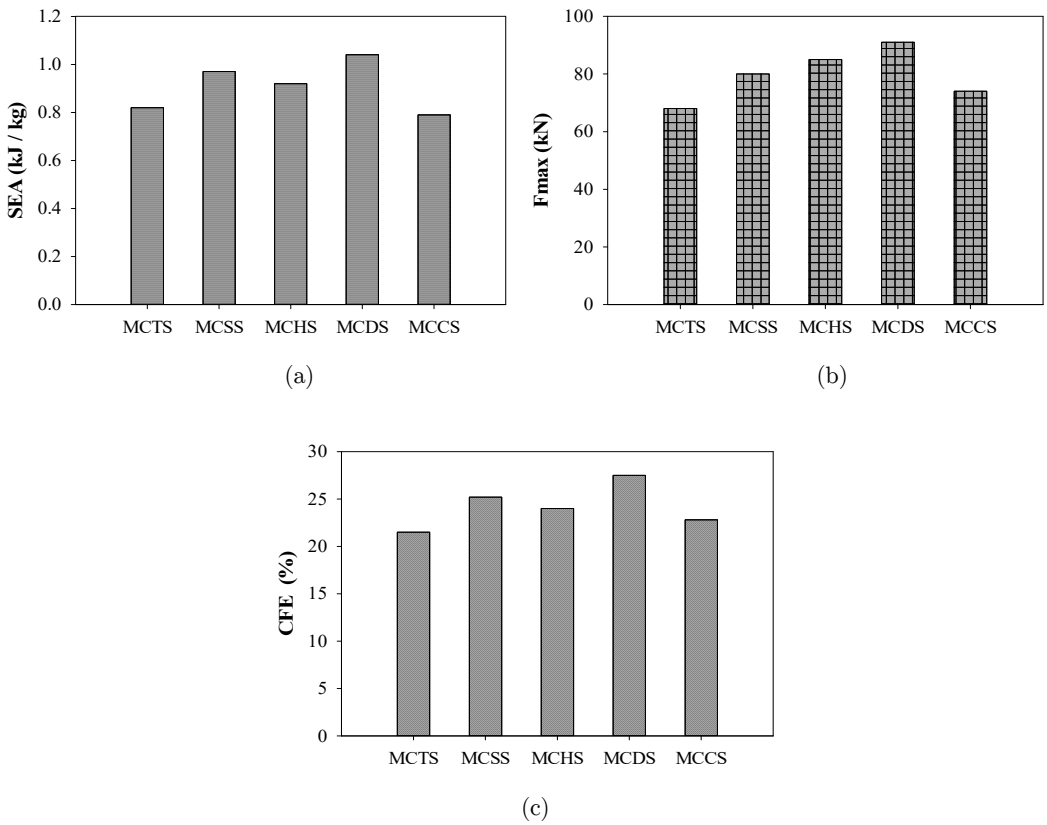

Figure 10: Crashworthiness indicators for the multi-cell S-rails: (a) SEA, (b) F_{max}, and (c) CFE.

4.4 Crashworthiness Comparison of the S-Rails Using the COPRAS Method

The multi criteria decision making method is applied in various situations where a number of alternatives need to be chosen. In this research, a multi-criteria decision making (MCDM) process known as the complex proportional assessment (COPRAS) developed by Zavadskas et al. (2007) and Zavadskas et al. (2008) was employed to select the better energy absorbers investigated in this research regarding the crashworthiness indicators calculated in the section 4.3. Actually, this is the ranking method which by considering conflicting criteria, the optimum alternative is selected. The steps to apply this method for the abovementioned results are explained below in detail.

Step 1: Construct the initial decision-making matrix, X as:

$$X = [X_{ij}]_{mn} = \begin{bmatrix} x_{11} & x_{12} & \dots & x_{1n} \\ x_{21} & x_{22} & \dots & x_{2n} \\ \dots & \dots & \dots & \dots \\ x_{m1} & x_{m2} & \dots & x_{mn} \end{bmatrix} \tag{5}$$

Where Xij is the performance value of ith criterion on j^{th} alternative. m and n state the number of criteria and alternatives, respectively.

Step 2: calculate the normalized initial decision-making matrix using:

$$R = [r_{ij}]_{mn} = \frac{X_{ij}}{\sum_{i=1}^{m} X_{ij}} \tag{6}$$

The purpose of normalizing the decision matrix is to find dimensionless values of different criteria for comparing all of them.

Step 3: Find the weighted normalized decision matrix, D as below:

$$D=[y_{ij}]_{mn} = r_{ij} \times W_j \tag{7}$$

Where r_{ij} is the normalized performance value of ith criterion on j^{th} alternative. W_i is the weight of ith criterion. The sum of dimensionless weighted normalized values of each criterion is always equal to the weight for that criterion:

$$\sum_{j=1}^{n} y_{ij} = W_i \tag{8}$$

In other words, the weight, w_i of the investigated criterion is proportionally distributed among all the alternatives according to their weighted normalized value, y_{ij}.

Step 4: The sums of weighted normalized values are calculated for both the beneficial criteria and non-beneficial criteria. The lower is the value of a non-beneficial criterion like F_{max} the better is the crashworthiness of the members. On the other hand, the greater is the value of a beneficial criterion like the SEA or CFE the better is the crashworthiness of the members. These sums are obtained as:

$$S_{+j} = \sum_{j=1}^{n} y_{+ij}$$
$$S_{-j} = \sum_{j=1}^{n} y_{-ij} \tag{9}$$

Where y_{+ij} and y_{-ij} are the weighted normalized values for the beneficial and non-beneficial criteria, respectively.

The greater the value of S_{+j}, the better is the alternative, and the lower the value of S_{-j}, the better is the alternative. The values of S_{+j} and S_{-j} state the degree of goals attained by each alternative. In any case, the sums of S_{+j} and S_{-j} of the alternatives are always respectively equal to the sums of weights for the beneficial and non-beneficial criteria as written by the following equations:

$$S_{+} = \sum_{j=1}^{n} S_{+j} \tag{10}$$

$$S_{-} = \sum_{j=1}^{n} S_{-j} \tag{11}$$

These equations can be used for verifying the calculations.

Step 5: characterize the significances of the alternatives based on defining the positive alternatives S_{+j} and negative alternatives S_{-j} characteristics.

Step 6: Determine the priorities of the alternatives. The priorities of the candidate alternatives are calculated based on Q_j written as:

$$Q_j = S_{+j} + \frac{S_{-\min} \sum_{j=1}^{n} S_{-j}}{S_{-j} \sum_{j=1}^{n} (1/S_{-j})} \quad (i = 1,2,...,n) \tag{12}$$

where $S_{-\min}$ is the minimum value of S_{-j}.

The greater the value of Q_j, the higher is the priority of the alternative. The relative significance value of an alternative states the degree of satisfaction achieved by that alternative. The alternative with the highest relative significance value ($Q_{\max}$) is the best choice among the all alternatives.

Step 7: Compute the quantitative utility (U_j) for j^{th} alternative. The degree of an alternative's utility is directly associated with its relative significance value (Q_j). The degree of an alternative's utility, leading to a complete ranking of the candidate alternatives, is determined by comparing the priorities of all the alternatives with the most efficient one and can be denoted as below (Mandal and Sarkar, 2012):

$$U_j = \frac{Q_j}{Q_{\max}} \times 100\% \tag{13}$$

Where $Q_{\max}$ is the maximum relative significance value. These utility values of the candidate alternatives range from 0% to 100%. Thus, this approach allows for evaluating the direct and proportional dependence of significance and utility degree of the considered alternatives in a decision-making problem involving multiple criteria, their weights and performance values of the alternatives with respect to all the criteria.

In order to select the suitable tube (among the tubes with different cross-sections illustrated in Fig. 2) in crashworthiness point of view, the complex proportional assessment (COPRAS) method was adopted. A good energy absorber must have greater SEA and CFE as well as less $F_{\max}$ to prevent the vehicle passengers from the severe damage during a crash. Therefore, all of the three crite-

ria (i.e. SEA, F_{max} and CFE) were required to be considered as the design criteria for comparing the S-rails.

COPRAS method was separately applied on the numerical results of both single-cell and multi-cell S-rails according to the procedures explained above. The decision matrix, normalized decision matrix, beneficial (S_{-i}) and non-beneficial(S_{+i}) attributes, relative significance or priority (Q) and quantitative utility (U) were computed as have been shown in Tables 1-2.

Section	F_{max}(kN)	SEA(kJ/kg)	CFE(%)
SCTS	25.41	0.639	28.2
SCSS	39.87	0.751	21.1
SCHS	41.69	0.813	22.1
SCDS	35.51	0.838	26.4
SCCS	28.81	0.689	26.8

(a)

Section	F_{max}(kN)	SEA(kJ/kg)	CFE(%)
SCTS	0.1482	0.1715	0.2265
SCSS	0.2325	0.2011	0.1695
SCHS	0.2436	0.2181	0.1767
SCDS	0.2074	0.2246	0.2119
SCCS	0.1682	0.1849	0.2153

(b)

Section	SCTS	SCSS	SCHS	SCDS	SCCS
S_+	0.1482	0.1545	0.1661	0.1772	0.1554
S_-	0.0296	0.0465	0.0487	0.0487	0.0336
Q_i	0.2105	0.1877	0.1978	0.214	0.199
U_i	93.90%	87.54%	92.24%	100%	93.23%
Rank	2	5	4	1	3
				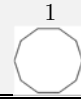	

(c)

Table 1: COPRAS results for the single-cell S-shaped members, (a) decision making matrix, (b) normalized decision making matrix, (c) ranking

From the COPRAS results presented in Tables 1-2, final ranking for the single-cell S-rails was obtained as SCDS, SCTS, SCCS, SCHS and SCSS; while the multi-cell S-shaped tubes were ranked as: MCDS, MCSS, MCHS, MCTS and MCCS. Therefore, the decagonal cross-section for both the single-cell and multi-cell S-rails was found the best cross-section shape to improve crashworthiness capability of the S-rails. It is worth noting that the mentioned ranking of the S-rails in terms of the crashworthiness capacity is only for the specified cross-sections illustrated in Figure 2. For example, the increase in the number of stiffener can result in increasing the F_{max}, the m (mass of the structure) and EA. Hence, SEA may not be increased because of increasing the m (or in the case of increasing the SEA, this increase may not compensate the increase of F_{max}). Because of this reason, complex conditions are created by increasing the number of stiffeners, and so any change in the cross-sectional configurations must be individually studied.

Section	F_{max}(kN)	SEA(kJ/kg)	CFE(%)
MCTS	69.19	0.821	22.8
MCSS	81.31	0.965	25.5
MCHS	83.48	0.928	23.3
MCDS	90.52	1.03	27.1
MCCS	73.51	0.804	22.9

(a)

Section	F_{max}(kN)	SEA(kJ/kg)	CFE(%)
MCTS	0.1741	0.1809	0.1957
MCSS	0.2045	0.2131	0.2097
MCHS	0.2101	0.2048	0.1916
MCDS	0.2271	0.2241	0.2138
MCCS	0.1844	0.1774	0.1891

(b)

Section	MCTS	MCSS	MCHS	MCDS	MCCS
S_+	0.1477	0.169	0.1612	0.1771	0.1443
S-	0.0348	0.0409	0.0421	0.0454	0.0369
Q_i	0.1932	0.2085	0.1989	0.2121	0.1873
U_i	91.11%	97.91%	94.1%	100%	88.31%
Rank	4	2	3	1	5
			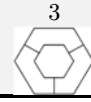	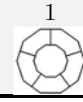	

(c)

Table 2: COPRAS results for the multi-cell S-shaped members, (a) decision making matrix, (b) normalized decision making matrix, (c) ranking

5 CRASH ANALYSIS OF S-RAILS WITH THE SAME OUTER TUBES AND DIFFERENT INNER ONES

According to the previous section, the multi-cell S-rail with decagon cross-section (MCDS) was found to perform as the best energy absorber. Thus, further analysis was carried out on this member by assuming the same outer cross-section (decagon) and changing the inner one to triangular, square, hexagonal, decagon and circular (see Figure 11). Number of the ribs was assumed as N=5 similar to the MCDS. Ratio of the inner tube perimeter to the outer one was also assumed equal with 0.5 like MCDS. Figure 12 exhibits deformation modes of these tubes. The corresponding force-displacement curves were also given in Figure 13. In addition, the crashworthiness indicators including SEA, F_{max} and CFE, calculated from the LS-DYNA, were presented in Figure 14.

Shape of cross-section		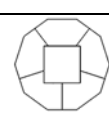	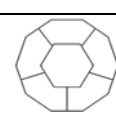	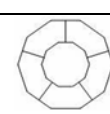	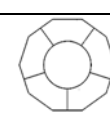
Designation	Type 1	Type 2	Type 3	Type 4	Type 5
Mass (kg)	9.53	9.44	9.38	9.25	9.19

Figure 11: Sectional schematic of the multi-cell S-rails.

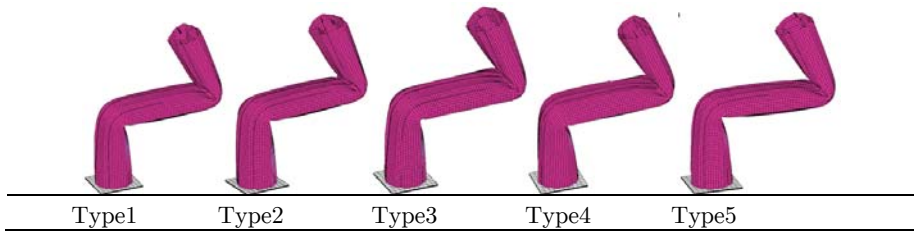

Figure 12: Deformation modes of the multi-cell S-rails.

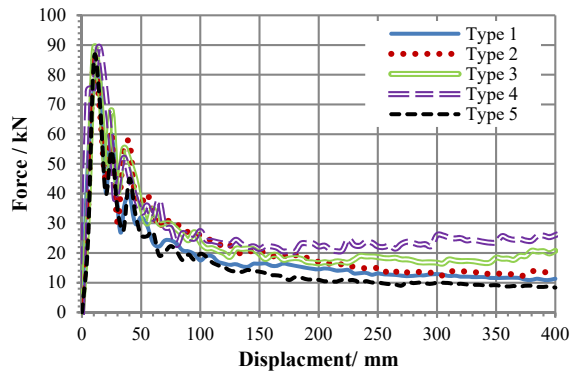

Figure 13: Force-displacement curves for the multi-cell S-rails.

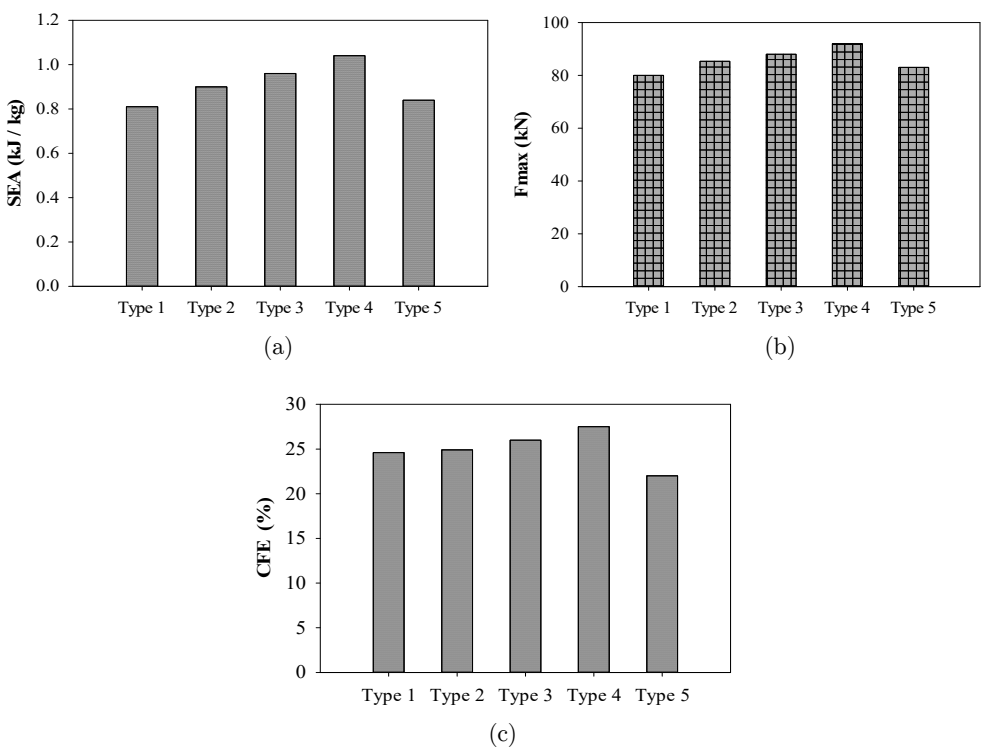

Figure 14: Crashworthiness indicators for the multi-cell S-rails: (a) SEA (b) F_{max} and (c) CFE.

COPRAS method was implemented on the results of these five tubes as is seen in Table 3. Based on the COPRAS calculations, the ranking was obtained as type 4>type 3>type 2>type 1>type 5. This signifies that the S-rail with the same outer and inner cross-section shape performed as the best energy absorbing device.

Section	F_{max}(kN)	SEA(kJ/kg)	CFE(%)
Type 1	81.19	0.831	24.6
Type 2	85.31	0.911	24.7
Type 3	87.18	0.941	25.2
Type 4	90.49	1.03	27.1
Type 5	85.31	0.842	22.5

(a)

Section	F_{max}(kN)	SEA(kJ/Kg)	CFE(%)
Type 1	0.1892	0.1832	0.2001
Type 2	0.1987	0.1987	0.2011
Type 3	0.2032	0.2075	0.2036
Type 4	0.2102	0.2252	0.2121
Type 5	0.1987	0.1854	0.1831

(b)

Section	Type 1	Type 2	Type 3	Type 4	Type 5
S_+	0.151	0.1595	0.1652	0.1774	0.1481
S_-	0.0378	0.0397	0.0406	0.042	0.0397
Q_i	0.1922	0.1996	0.2045	0.2155	0.1881
U_i	89.2%	92.64%	95.2%	100%	87.31%
Rank	4	3	2	1	5
			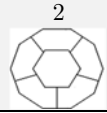	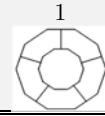	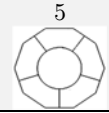

(c)

Table 3: COPRAS results for the S-rails with the same outer cross-section and different inner one, (a) decision making matrix, (b) normalized decision making matrix, (c) ranking.

6 PARAMETRIC STUDY

According to the previous section, the multi-cell S-rail with decagonal cross-section and five ribs (namely MCDS member) was identified as the best alternative for dissipating collision energy. A parametric study was performed to evaluate effects of the geometrical parameters on the crashworthiness capacity of the selected S-rail (MCDS). These parameters consisted of the wall thickness t, curve angle ϑ, and the perimeter ratio S (see Table 4). These parameters namely t, ϑ and S were varied to be 2, 2.5, 3 and 3.5 mm, 30°, 40°, 50° and 60°, 0.3, 0.45, 0.6 and 0.7, respectively. The S-rails with these geometries were modeled and analyzed in LS-DYNA (according to the notes and values mentioned in the section 4.1), and the corresponding results for the SEA, F_{max} and CFE were computed as are seen in Table 5. The material properties were similar to the ones mentioned in the section 2. Variations of the SEA, F_{max} and CFE against the parameters of S and ϑ for the wall

thickness of t=2, 2.5, 3, 3.5 have been plotted in Figure 15-17, respectively. As is evident from these figures, by increasing the wall thickness (while S and ϑ were considered to be constant), the values of SEA and F_{max} increased.

Parameters	lower bound	upper bound	step size
Wall thickness (t/mm)	2	3.5	0.5
Perimeter (radius) ratio (S)	0.3	0.75	0.15
Curve angle (ϑ/ º)	30	60	10
Geometry	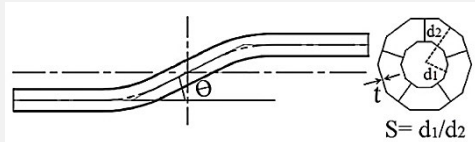		

Table 4: Geometrical parameters, range and step size for the parametric study of the multi-cell S-rails with decagonal cross-section.

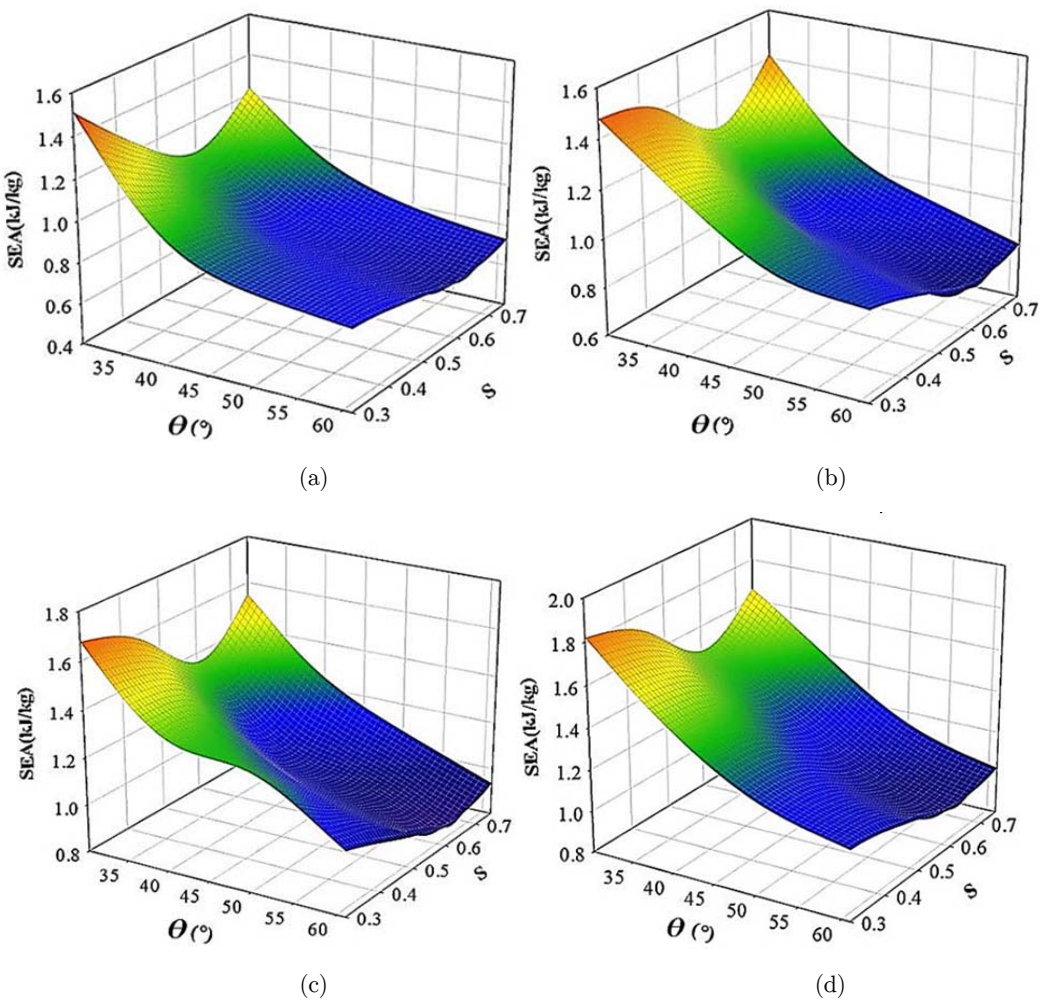

Figure 15: Variations of SEA against ϑ & S for the MCDS S-rails with different thicknesses of (a) t=2, (b) t=2.5, (c) t=3, (d) t=3.5.

	Design parameters				Criteria		
NO	ϑ (º)	S	t(mm)	W(kg)	F_{max}(kN)	SEA(kJ/kg)	CFE (%)
1	30	0.3	2	5.76	124.31	1.5121	17.51
2	30	0.45	2	5.87	125.27	1.2248	14.34
3	30	0.6	2	5.98	129.75	1.0451	12.04
4	30	0.75	2	6.09	146.25	1.2331	12.83
5	30	0.3	2.5	7.21	149.11	1.4785	17.87
6	30	0.45	2.5	7.34	171.94	1.4087	15.03
7	30	0.6	2.5	7.48	163.43	1.2125	13.87
8	30	0.75	2.5	7.6	190.12	1.4184	14.17
9	30	0.3	3	8.65	145.6	1.6786	24.93
10	30	0.45	3	8.81	217.44	1.5766	15.96
11	30	0.6	3	8.97	204.21	1.3634	14.97
12	30	0.75	3	9.14	220.21	1.5503	16.1
13	30	0.3	3.5	10	157.63	1.8203	28.86
14	30	0.45	3.5	10.28	215.21	1.7140	20.46
15	30	0.6	3.5	10.47	225.23	1.4794	17.19
16	30	0.75	3.5	107	230.4	0.1654	19.2
17	40	0.3	2	5.92	55.32	1.0084	26.98
18	40	0.45	2	6.03	60.88	0.9286	22.99
19	40	0.6	2	6.14	56.12	0.8061	22.05
20	40	0.75	2	6.25	65.86	0.9312	22.09
21	40	0.3	2.5	7.3	80.81	1.2287	27.75
22	40	0.45	2.5	7.54	92.54	1.1405	23.23
23	40	0.6	2.5	7.68	78.12	0.9518	23.39
24	40	0.75	2.5	7.82	89.11	1.0767	23.62
25	40	0.3	3	8.88	109.15	1.3547	27.55
26	40	0.45	3	9.05	110.31	1.2850	26.35
27	40	0.6	3	9.22	98.41	1.0726	25.12
28	40	0.75	3	9.38	122.22	1.2473	23.93
29	40	0.3	3.5	10.36	146.3	1.4835	26.26
30	40	0.45	3.5	10.56	132.52	1.4346	28.58
31	40	0.6	3.5	10.75	124.92	1.2818	27.58
32	40	0.75	3.5	10.97	146.31	1.3855	25.97
33	50	0.3	2	6.06	49.82	0.8465	25.74
34	50	0.45	2	6.2	44.50	0.8129	28.31
35	50	0.6	2	6.3	48.20	0.7142	23.34
36	50	0.75	2	6.42	68.33	0.7943	18.66
37	50	0.3	2.5	7.57	62.65	1.0224	30.88
38	50	0.45	2.5	7.74	72.53	0.9767	26.05
39	50	0.6	2.5	7.88	54.55	0.8426	30.43
40	50	0.75	2.5	8.02	74.92	0.9339	24.99
41	50	0.3	3	9.09	81.58	1.2981	36.16
42	50	0.45	3	9.28	89.41	1.1034	28.61
43	50	0.6	3	9.46	86.22	0.9735	26.71
44	50	0.75	3	9.62	103.51	1.0810	25.12
45	50	0.3	3.5	10.6	113.62	1.2481	29.11
46	50	0.45	3.5	10.83	114.46	1.2086	28.59
47	50	0.6	3.5	11.04	93.77	1.0597	31.19

48	50	0.75	3.5	11.2	123.2	1.1446	26.01
49	60	0.3	2	6.23	30.41	0.7993	40.95
50	60	0.45	2	6.35	43.39	0.7574	27.71
51	60	0.6	2	6.45	62.59	0.6356	16.37
52	60	0.75	2	6.6	35.60	0.7318	33.91
53	60	0.3	2.5	7.78	48.26	0.9730	39.21
54	60	0.45	2.5	7.9	46.96	0.8924	37.53
55	60	0.6	2.5	8.08	55.20	0.7413	27.12
56	60	0.75	2.5	8.23	55.42	0.8262	30.68
57	60	0.3	3	9.3	66.40	1.0946	38.32
58	60	0.45	3	9.52	78.21	1.0094	30.72
59	60	0.6	3	9.7	50.93	0.8422	40.12
60	60	0.75	3	9.88	76.78	0.9352	30.08
61	60	0.3	3.5	10.9	84.69	1.1431	36.77
62	60	0.45	3.5	11.1	95.09	1.0954	31.66
63	60	0.6	3.5	11.3	75.60	0.9407	35.15
64	60	0.75	3.5	11.53	95.71	1.0234	30.82

Table 5: Crashworthiness indicators of the multi-cell S-rails with decagonal cross-section at the design points.

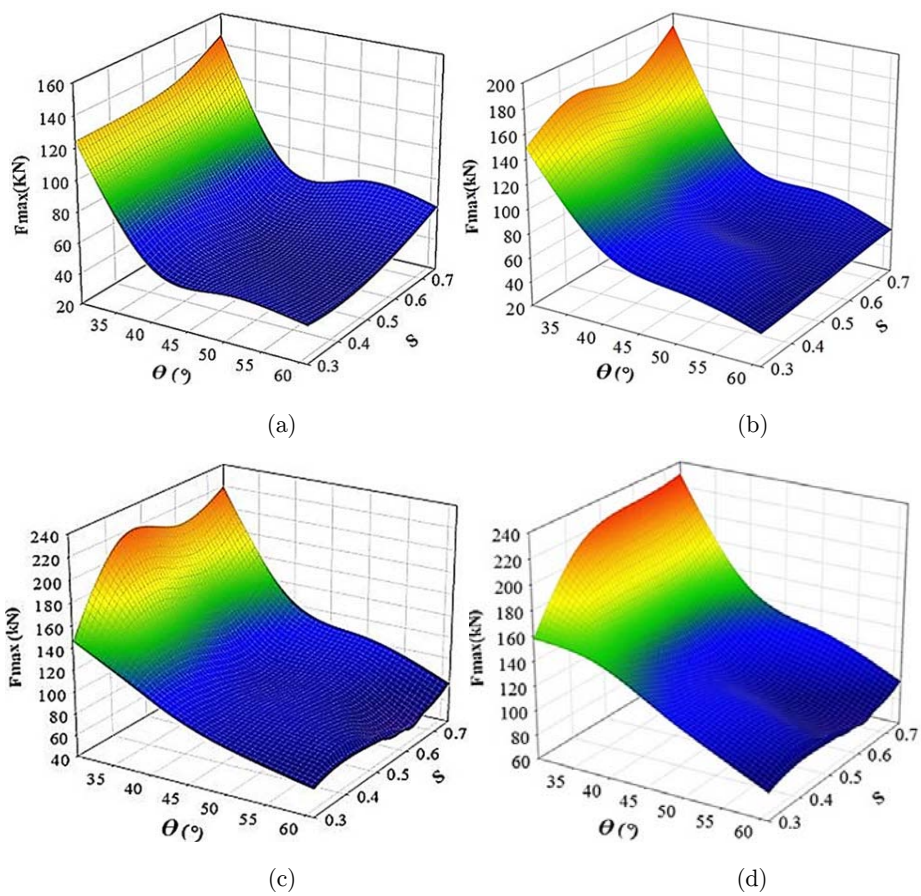

Figure 16: Variations of SEA against ϑ & S for the MCDS S-rails with different thicknesses of (a) t=2, (b) t=2.5, (c) t=3, (d) t=3.5.

It is obvious in Figure 15 that as the perimeter ratio S increased, SEA initially reduced up to S=0.6 and then increased. Furthermore, SEA had the maximum value at S=0.3. On the other hand, by increasing the perimeter ratio S, the peak force F_{max} enhanced and CFE decreased (see Figure 16-17). It is also clear from these figures that as the curve angle ϑ increased, SEA initially reduced and then remained approximately unchanged. This behavior of the S-rails corresponds to changing progressive folding collapse mode to the global bending. Moreover, by increasing the curve angle ϑ, generally both the peak force F_{max} and CFE decreased.

The COPRAS method was finally implemented on the results presented in Table 5 considering three crashworthiness criteria namely SEA, F_{max} and CFE. This calculations lead to find the optimum geometrical parameters of S-rail as: ϑ=60°, S=0.3 and t=2 mm. The results reveal that, the optimum values have been taken place at the upper or lower bounds. These values are indeed the usual values taken in the literatura (khalkhali, 2015; Elmarakbi et al., 2013; Han and Yamazaki, 2001; Kim et al., 2002). It is evident that changing the lower and upper bounds would probabaly give different results.

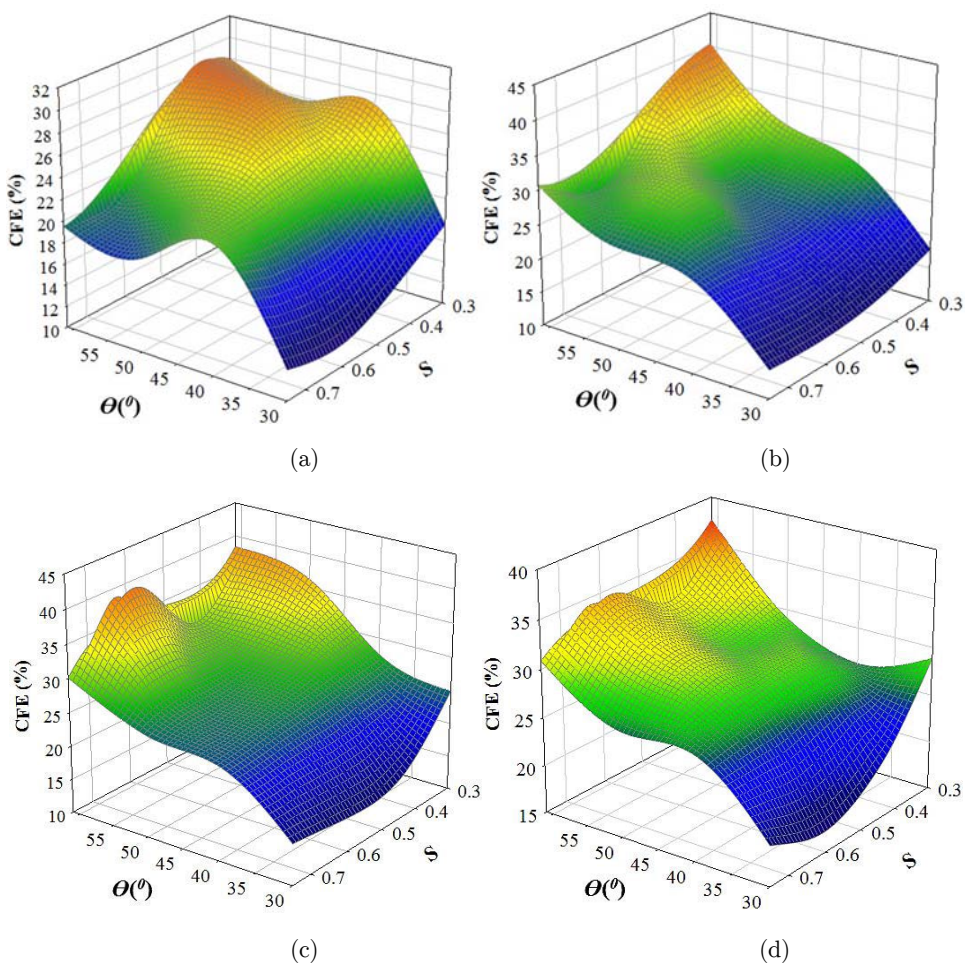

Figure 17: Variations of CFE against ϑ & S for the MCDS S-rails with different thicknesses of (a) t=2, (b) t=2.5, (c) t=3, (d) t=3.5.

7 CONCLUSIONS

In this research, crashworthiness performance of S-shaped members with different cross-sections was numerically studied under axial crash. The following important results were drawn:

- Single-cell and multi-cell S-rails with triangular, square, hexagonal, decagon and circular cross-sections were analyzed in LS-DYNA, and three main crashworthiness indicators i.e. SEA, F_{max} and CFE were computed. In order to select the suitable tube among these S-rails, the COPRAS method was applied on the numerical results. The proposed multi-cell S-rail with decagonal cross-section was finally found to be the best energy absorbing device.
- Double-walled S-rails with the same outer cross-section (decagonal) and different inner one (i.e. triangular, square, hexagonal, decagon and circular) were also investigated from the crashworthiness point of view. The results demonstrated that the S-rail with the same outer and inner cross-section (decagonal) had the best crashworthiness performance using the COPRAS method.
- Parametric study was performed on the aforementioned selected S-rail to evaluate effects of the geometrical parameters including the wall thickness t, curve angle ϑ, and the perimeter ratio S (each one at four levels) on the crashworthiness capacity. COPRAS calculations lead to find the optimum geometrical parameters of S-rail as: ϑ=60°, S=0.3 and t=2 mm.

References

Abe, K. Nishigaki, K., Ishivama, S., Ohta, M., Takagi, M., Matsukawa, F., (1990). Collapseof thin- walled curved beam with closed-hat section-part 2: Simulation by plane plastic hinge model. SAE Technical Paper 10, 900461.

Ahmed, E. Yee, X.L. John, M., (2013) .Crash analysis and energy absorption characteristics of S-shape longitudinal members. Thin-Walled Structures 68: 65–74.

AlaviNia, A. Parsapour, M., (2014). Comparative analysis of energy absorption capacity of simple and multi-cell thin-walled tubes with triangular, square, hexagonal and octagonal sections. Thin-Walled Structures 74: 155–165.

Atahan, A.O. Yucel, A.O. Erdem, M., (2014). Crash testing and evaluation of a new generation L1 containment level guardrail. Engineering Failure Analysis 38: 25−37.

Belingardi, G. Boria, S. Obradovic, J., (2013). Energy absorbing sacrificial structures made of composite materials for vehicle crash design. Dynamic Failure of Composite and Sandwich Structures. 192: 577−609.

Chen, W. (2001) Experimental and numerical study on bending collapse of aluminum foam-filled hat profiles. International Journal of Solids and Structures 38: 7919-7944.

Chen, W. Wierzbicki, T., (2001). Relative merits of single-cell, multi-cell and foam- filled thin-walled structures in energy absorption. Thin-Walled Structures 39(4):287–306.

Cheon S.S. Meguid, S.A., (2004) .Crush Behavior of Metallic Foams for Passenger Car Design. International Journal of Automotive Technology 5: 47-53.

Elmarakbi, A. Fielding, N. Hadavinia, H., (2011). Finite element simulation of the axial crush of thin-walled tubes with different cross-sections: vehicle/ pole impact application. International Journal of Vehicle Structures & Systems 3:154–60.

Elmarakbi, Ahmed. Long, Y.X., MacIntyre, J., (2013). Crash analysis and energy absorption characteristics of S-shaped longitudinal members. Thin-Walled Structures 68:65–74.

Han, J. Yamazaki, K., (2001) A study on the crashworthiness of S-shape square tubes, Transactions on the Built Environment 52, ISSN 1743-3509.

Han, J. Yamazaki, K., (2003) Crashworthiness Optimization of S-shape Square Tubes. International Journal of Vehicle Design 31: 72-85.

Hong, H.-W. Fan, Z.-J. Yu, G. Wang, Q.-Ch, Tobota, A., (2005). Partition energy absorption of axially crushed aluminum foam-filled hat sections International Journal of Solids and Structures 42: 2575-2600.

Hosseini-Tehrani, P. Nikahd, M., (2006). Effects of ribs on S-frame crashworthiness. Proceeding of IMechE Part D: J of Automobile Eng 220: 1679–89.

Hosseini-Tehrani, P. Nikahd, M., (2006). Two materials S-frame representation for improving crashworthiness and lightening. Thin-Walled Structures 44: 407–14.

Khalkhali, A. Agha Hossinali Shirazi, V. Mohseni Kabir, M., (2013). Closed-form solution for peak crushing force of the S-rails [J]. International Journal of Automotive Technology 3: 446—456.

Khalkhali, A. Darvizeh, A. masoumi, A. Nariman-Zadeh, N., (2011). Experimental and numerical investigation into the quasi-static crushing behaviour of the S-shape square tube International Journal of Mechanical Sciences 27:585—596.

Khalkhali, A., (2015). Best compromising crashworthiness design of automotive S-rail using TOPSIS and modified NSGAII. Journal of Central South University 22: 121—133.

Kim, H.S. Chen, W. Wierzbicki, T., (2002). Weight and crash optimization of foam-filled three-dimensional S frame. Computational Mechanics. 28: 417–24.

Kim, H.S. Wierzbicki, T., (2000). Effect of the cross-sectional shape on crash behavior of a 3-D space frame [R]. Impact and Crashworthiness Laboratory Report No. 34, MIT.

Kim, H.S. Wierzbicki, T., (2004). Closed-form solution for crushing response of three-dimensional thin-walled S frames with rectangular section. International Journal of Impact Engineering 30: 87—112.

Langseth, M. Hopperstad, O.S., (1996). Static and dynamic axial crushing of square thin-walled aluminium extrusions. International Journal of Impact Engineering 18(7–8):949-968.

Li, Q.M. Mines, R.A.W. Birch, R.S., (2000).The crush behaviour of Rohacell-51WF structural foam. International Journal of Solids and Structures 37: 6321-6341.

Mandal, U.K. Sarkar, B. A., (2012). Exploratory analysis of intelligent manufacturing system (Ims) under fuzzy utopian environment. IOSR J of Eng 2: 129-140.

Marsolek, J. Reimerdes, H.G., (2004). Energy absorption of metallic cylindrical shells with induced non-axisymmetric folding patterns. . International Journal of Impact Engineering 30:1209–23.

Ohkami, Y. Takada, K. Motomura, K. Shimamura, M., (1990). Tomizawa H, Usuda M. Collapse of thin-walled curved beam with closed-hat section-part 1: study on collapse characteristics. SAE Technical Paper. 10, 900460.

Pawlus, W. Karimi, H.R. Robbersmyr, K.G., (2011). Mathematical modeling of a vehicle crash test based on elasto-plastic unloading scenarios of spring-mass models. The International Journal of Advanced Manufacturing Technology 55: 369—378.

Reyes, A. Hopperstad, O.S. Langseth, M., (2004). Aluminum foam-filled extrusions subjected to oblique loading: experimental and numerical study. International Journal of Solids and Structures 41:1645-1675.

Zavadskas, E.K. Turskis, Z. Tamošaitiene, J. Marina, V., (2008). Multi criteria selection of project managers by applying grey criteria. Technology and Economic Development 14: 462–77.

Zhang, C. (2005). Study of Crash Behavior of a 3-D S-Shape Space Frame Using Finite Element Method. M.S. Thesis, Tufts University, Medford.